THE JOURNAL OF PHYSICAL CHEMISTRY C

Article

pubs.acs.org/JPCC

Toward Stronger Al−BN Nanotube Composite Materials: Insights into Bonding at the Al/BN Interface from First-Principles Calculations

Arkady V. Krasheninnikov,*[,†] Natalia Berseneva,[‡] Dmitry G. Kvashnin,[§] Jussi Enkovaara,[‡,∥] Torbjörn Björkman,[‡] Pavel Sorokin,[§,⊥,#] Dmitry Shtansky,[§] Risto M. Nieminen,[‡,∇] and Dmitri Golberg[○]

[†]Department of Applied Physics, Aalto University, P.O. Box 11100, FI-00076 Aalto, Finland

[‡]COMP Centre of Excellence, Department of Applied Physics, Aalto University, P.O. Box 11100, FI-00076 Aalto, Finland

[§]National University of Science and Technology "MISiS", Leninsky pr. 4, Moscow 119049, Russian Federation

[∥]CSC-IT Center for Science Ltd., FI-02101 Espoo, Finland

[⊥]Technological Institute for Superhard and Novel Carbon Materials,7a Centralnaya Street, Troitsk, Moscow 142190, Russian Federation

[#]Moscow Institute of Physics and Technology, 9 Institutsky Lane, Dolgoprudny 141700, Russian Federation

[∇]Dean's Office, Aalto University School of Science, P.O. Box 11000, 00076 Aalto, Finland

[○]World Premier International Center (WPI) for Materials Nanoarchitectonics (MANA), National Institute for Materials Science (NIMS), Namiki 1-1, Tsukuba, Ibaraki 3050044, Japan

ABSTRACT: Lightweight mechanically strong composite Al/BN nanotube materials may find applications in the automotive and space industries because addition of a few percent of the nanotubes considerably improves the mechanical properties of the Al matrix. At the same time, experiments indicate that bonding at the interface between Al and the nanotubes is rather weak, which limits the performance of the composites. To get precise microscopic knowledge of the atomic structure and bonding at the interface between the Al matrix and BN nanotubes and to suggest ways to improve the adhesion, we employ density functional theory with van der Waals exchange−correlation functionals and carry out first-principles calculations of the interface between the Al(111) surface and hexagonal BN sheets, mimicking BN nanotubes with large diameters. We estimate the bonding energy and the interfacial critical shear stress and compare the theoretical results to the experimental data. We further assess how point defects, such as atomic vacancies and substitutional impurities, affect the interface bonding. We show that some point defects (e.g., single B vacancies) dramatically change the atomic structure of the interface, giving rise to stronger bonding and higher critical shear stress values. Larger vacancies and substitutional C impurities in the BN sheets have a stronger effect on the adhesion. Finally, we demonstrate that even though defects deteriorate the mechanical properties of BN nanotubes, this effect is rather weak at defect concentrations of a few percent, so that an overall improvement of the characteristics of Al/BN nanotube composites after introduction of defects at the interface can be expected. We suggest possible routes for the development of nanostructured BN−Al materials with improved mechanical characteristics.

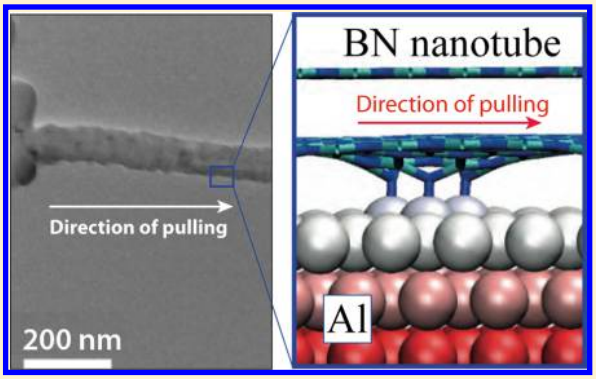

INTRODUCTION

The development of lightweight but mechanically strong materials is crucial for the automotive and space industry, associated with an increase in payload, improvement of fuel efficiency, decrease in pollution, and overall usage cost reduction. Mostly Al-based materials (especially Al-based alloys) are in use now, providing a reasonable compromise between the cost and material strength. Nevertheless, mechanical characteristics of such materials are quite moderate. For example, pure Al has relatively small values of Young's modulus and tensile strength, about 70 GPa and 40 MPa, respectively.[1,2] Moreover, heating to temperatures of only 200 °C gives rise to further decrease in these characteristics. Thus, the need for finding ways to make Al tougher and stiffer has been the driving force for extensive research in this area.[2]

One of the suggested ways to improve the mechanical characteristics of Al-based materials is to reinforce[3−5] the Al matrix by adding a few percent of carbon[6] or boron-nitride[7] nanotubes (BNNTs). BNNTs have extremely high Young's modulus (about 1 TPa), similar to that of carbon nanotubes, and are chemically inert, but contrary to the latter, are straight and do not stick together, thus providing a spatially uniform

Received: September 19, 2014
Revised: October 24, 2014
Published: October 28, 2014

   dx.doi.org/10.1021/jp509505j | J. Phys. Chem. C 2014, 118, 26894−26901

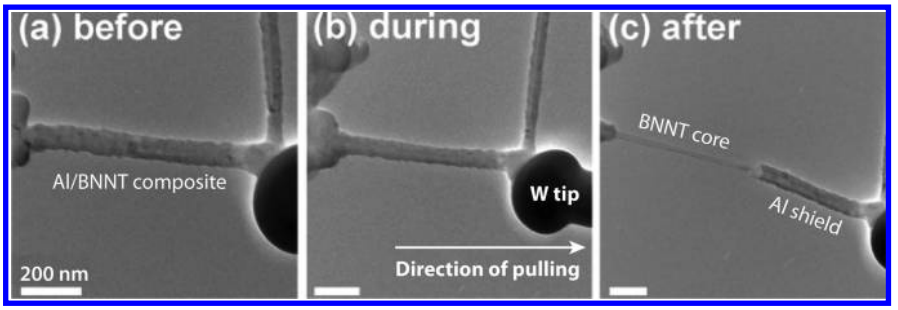

Figure 1. TEM images of an Al−BNNT nanocomposite under in situ TEM tensile testing. The multiwalled BNNT core (~50 nm in diameter) was coated with a ~20 nm layer of Al under magnetron sputtering (a). The tungsten tip is moved in the direction of the arrow. During a tensile test (b), the inner core is seen to be pulled out of the Al shield (c), implying a weak cohesion force between the BN core and metallic coating. This limits the nanocomposite mechanical reinforcement and an efficient load transfer from the soft Al to strong BN tube.

distribution, which is a severe problem in carbon-nanotube/Al composite materials.[8,9] Indeed, earlier experiments[10] showed that samples of composite materials based on melt-spun aluminum matrix reinforced by BN nanotubes had a tensile strength of 145 MPa, which is 2.5 times higher than nonreinforced aluminum ribbons prepared at the same casting conditions. Composite samples on the basis of aluminum containing only 3 wt % of BN nanotubes and produced via a high-pressure torsion demonstrated the tensile strength at room temperature of 350 MPa,[11] which is already comparable with the strength of some structural steels, but the composite material is nearly three times lighter. These results had demonstrated good prospects for using BN nanosystems for reinforcement of light metal matrices and achieving novel ultralight and superstrong composites.

The characteristics of the composite materials could have been considerably better, though, taking into account the outstanding mechanical properties of BNNTs. Transmission electron microscopy (TEM) experiments[9] indicated that the "bottleneck" is a weak bonding at the Al/BNNT interface, so that improving the adhesion between the Al matrix and BNNTs is the key issue. The progress here is, however, hardly possible without precise microscopic knowledge of the atomic structure of the interface. At the same time, very little is known about the morphology of the interface between BNNT (or hexagonal BN sheets, h-BN) and Al. This is in a sharp contrast to the large body of experimental and theoretical data on the interface between BN sheets and transition metals, as the latter have been extensively used for growing two-dimensional h-BN sheets.[12−17] In addition to the experimental characterization of the interface between BN sheets and transition metals by various techniques, significant insight into the atomic structure of the interface has been obtained from first-principles atomistic simulations (see ref 18 for an overview and references therein).

By carrying out first-principles density-functional theory (DFT) calculations, we theoretically study the bonding between pristine BN nanotubes and ideal Al matrix. We estimate the bonding energy and the critical shear stress and compare the theoretical results to the experimental data. We further assess how point defects such as atomic vacancies and substitutional impurities affect the interface bonding. We show that some, but not all, point defects (e.g., single B vacancies) dramatically change the interface structure and increase the bonding as well as critical shear stress. Larger vacancies and substitutional C impurities in the BN sheets have a stronger effect on the adhesion, suggesting possible routes for the development of nanostructured BN−Al materials with improved mechanical characteristics.

EXPERIMENTS ON THE TENSILE TESTING OF AL−BNNT NANOCOMPOSITES

The mechanical properties of individual Al matrix-BNNT nanohybrids have been previously studied at length by tensile tests using a combination of in situ transmission electron−atomic force microscopy (TEM−AFM).[9] All the details of Al−BNNT material synthesis, characterization, and testing are given in previous publications,[10,11] so that here we just show a typical picture of the evolution of the system during the tensile tests, which motivated our theoretical studies.

Figure 1 presents TEM images of an Al−BNNT nanocomposite under in situ TEM tensile testing. The multiwalled BNNT (~50 nm in diameter) was coated with a ~20 nm layer of Al under magnetron sputtering, Figure 1a. During a tensile test, Figure 1b, the BNNT was pulled out of the Al shield, Figure 1c, implying a weak cohesion force between the BN core and metallic coating. The weak bonding and apparent low tensile strength at the interface (of the order of 50 MPa) limits the nanocomposite mechanical reinforcement and an efficient load transfer from the soft Al to strong BN tube.

COMPUTATIONAL DETAILS

To get microscopic insights into the atomic structure of the interface, we carried out first-principles DFT calculations using the plane-wave-basis-set Vienna ab initio simulation package.[19,20] The projector augmented wave method[21] was used to describe the core electrons, and several exchange and correlation (XC) functionals including the nonlocal van der Waals (vdW) component[22,23] were employed. A plane wave kinetic energy cutoff of 400 eV was found to converge the total energy within 0.1 eV, as test calculations with higher cutoff energy of 500 eV showed. The same accuracy was achieved with regard to the number of k-points ($3 \times 3 \times 1$) in the two-dimensional Brillouin zone of the supercell. All structures were relaxed until atomic forces were below 0.002 eV/Å. We also did similar calculations for the interface between pristine Al and h-BN systems using the code GPAW[24] and the vdW-DF XC functional.[25] The spacing of the real-space grids was chosen to be 0.2 Å in all calculations. Simulations with smaller grids gave essentially the same results.

As the typical diameter of multiwalled BNNT used in experiments is rather large, about 50 nm, and because BNNTs are known to undergo polygonization[26] resulting in the flattening of the shells, we modeled the interface between

dx.doi.org/10.1021/jp509505j | J. Phys. Chem. C 2014, 118, 26894−26901

BNNTs and Al as that between a h-BN sheet and densely packed low-energy (111) Al surface, as schematically shown in Figure 2.

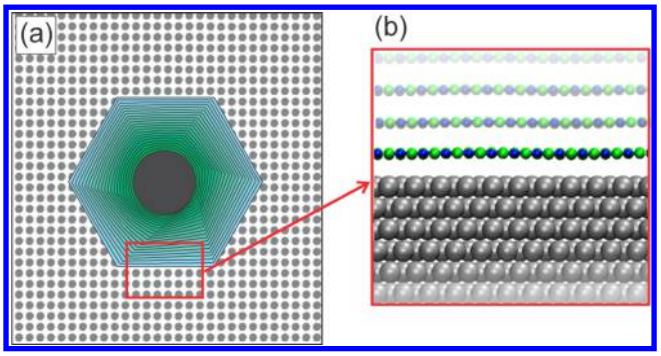

Figure 2. Schematic representation of a multiwalled BN nanotube embedded into Al matrix (a) and the atomistic picture of the BN−Al interface (b). Gray balls stand for aluminum atoms, blue for nitrogen, and green for boron.

The calculations were carried out for a 128-atom 8 × 8 h-BN supercell on top of a 7 × 7 three-atomic-layer-thick Al(111) slab containing 147 atoms. Such a periodic supercell resulted in a very small strain (introduced into the Al system) of 0.28%. To separate the periodic images of the sla, 20 Å of vacuum was added in the transverse direction. The bottom layer metal atoms were kept fixed in the positions corresponding to those in the bulk system. A similar simulation setup has been used before to model the graphene/Ir interface.[27−29]

In addition, to test the vdW exchange−correlation functional used, and to compare bonding at the h-BN/Al interface to that at the h-BN/typical transition metal, we also carried out simulations of the h-BN/Ru interface. The h-BN/Ru supercell consisted of 432 Ru atoms (12 × 12 three-atomic-layer-thick slab with the (0001) surface) and a 338-atom 13 × 13 h-BN sheet.

RESULTS

Bonding at the Interface between h-BN and Al/Ru in the Absence of Defects. The atomic structures of the interface between an h-BN sheet and Al(111) as well as Ru(0001) surfaces are shown in Figure 3. Metal atoms are depicted as balls, and the atomic network of h-BN sheets is presented as sticks. The h-BN atomic network is colored according to the elevation above the surface of the metal, with blue indicating "high" and red indicating "low". The PW86R-based VV10sol XC functional[23] was used. It is evident that the vdW interaction between the h-BN and the metal surface gave rise to the development of moiré superstructures with a corrugation of 1.8 Å for Ru and 0.3 Å for Al. We calculated the total binding energy defined as

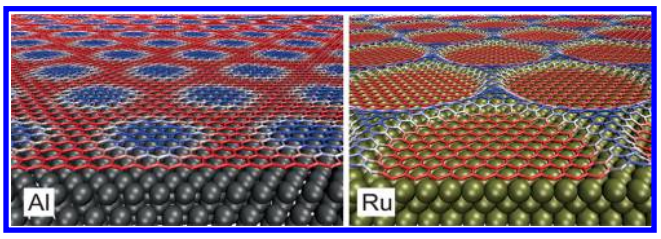

Figure 3. Atomic structure of the interface between h-BN and Al(111) (left panel) and Ru(0001) (right panel) surfaces. Metal atoms are shown as balls, and the atomic network of the h-BN sheet is presented as sticks. The h-BN atomic network is colored according to the elevation with regard to the surface of the metal, with blue color indicating "high" and red indicating "low". The difference in the moiré superstructures developed because of the interaction between the metals, and h-BN is evident. Note that the color scheme is different: while for Al the difference between the maximum and minimum elevation of B/N atoms is 0.3 Å, it is 1.8 Å in the case of Ru.

$$E_b^{tot} = E[M + BN] - (E[M] + E[BN]) \quad (1)$$

where E[M+BN], E[M], and E[BN] are the total energies of the combined metal/h-BN system, isolated metal slab, and h-BN sheet, respectively; M = Al or Ru. The binding energy per area unit was found to be E_b = 13.5 meV/Å^2 for Al and 66 meV/Å^2 for Ru.

For the h-BN/Ru system, similar moiré patterns have been reported.[18] The calculated values of the interaction energies also agree well with the results of previous calculations (~55 meV/Å^2).[18] E_b is considerably larger than the typical vdW energies,[30] indicating a weak covalent interaction between Ru(0001) and h-BN. On the basis of the good agreement between the results of our calculations and previously reported experimental and theoretical data, one can conclude that our computational approach is an adequate method for studying the h-BN/metal interfaces.

The interaction between Al and h-BN is much weaker than for Ru: calculations using the AM05-based,[23] PW86R-based VV10sol,[23] VV10,[22] and vdW-DF[25] XC functionals gave 13.6, 13.7, 21.1, and 16.3 meV/Å^2 respectively. The low values of E_b as well as the analysis of the spatial distribution of the electron density indicated that the interaction between Al and h-BN is of vdW type only. Two different configurations were considered (a B atom exactly on top of the surface Al atom in the HCP configuration and an N atom in the position, see Figure 4 and the corresponding discussion), but the results proved to be the same within 0.1 meV/Å^2. All the XC correlation functionals gave qualitatively the same moiré pattern.

Having evaluated the interaction energy between h-BN and Al surface, we moved on to the calculations of the critical shear stress, τ_c. This quantity is used in essentially all analytical models of composite materials.[3] In practice, the h-BN sheet was moved stepwise along the supercell axes and the supercell diagonal, Figure 4, and for each position the total energy was calculated. During geometry optimization, the B and N atoms were allowed to move in the transverse direction only. Then the maximum force along the path, and correspondingly τ_c defined as the maximum force divided by the interface area, was numerically evaluated. Depending on the XC functional used, calculations gave values of τ_c in the range of 8−17 MPa. These are very low values consistent with our experimental findings.

Bonding at the h-BN/Al Interface with N and B Single Vacancies. Point defects are ubiquitous and can easily be created at the h-BN/Al interface during the synthesis of the composite material. One can expect that defects affect the h-BN/Al interface structure and bonding, similar to the interface between h-BN[31] or graphene[28] and transition metals. Moreover, as defects in carbon nanotubes have been reported to be the preferential sites for polymer attachment[32] making the nanotube-polymer composites stronger, some defects may be beneficial for h-BN/Al composites.

We started our analysis by considering B and N vacancies in a h-BN sheet. Normally, the energetics of the system with

dx.doi.org/10.1021/jp509505j | J. Phys. Chem. C 2014, 118, 26894−26901

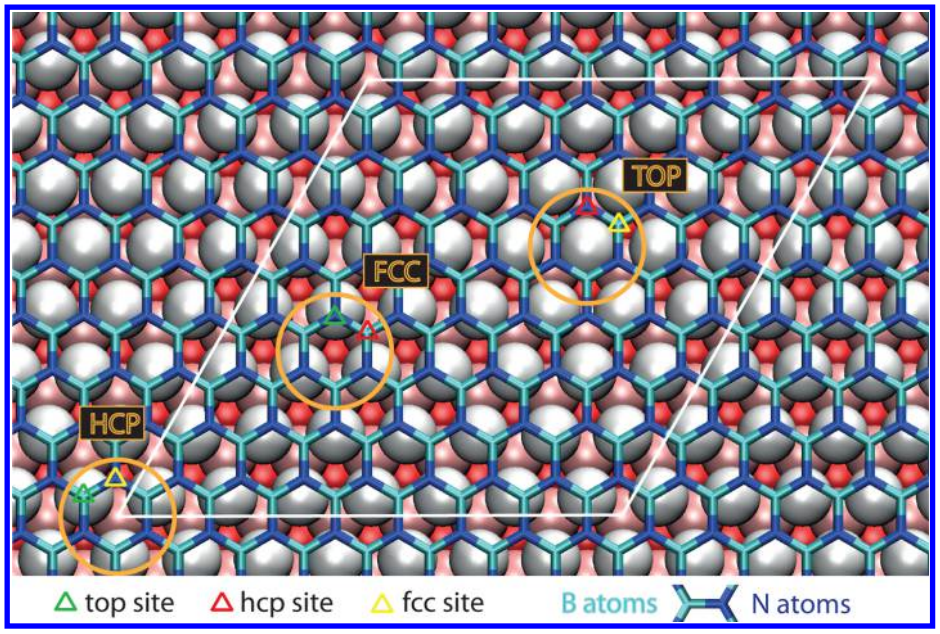

Figure 4. High-symmetry atomic positions at the interface between h-BN and Al(111). Al atoms are represented as balls colored according to the layers they are in with regard to the surface. The centers of BN-hexagons can be associated with the HCP, FCC positions in the underlying Al lattice as well as with the TOP position (on top of a surface Al atom). The supercell is shown with white lines. Vacancies in the high-symmetry areas can be created by removing B and N atoms which are in the hcp, fcc, and top positions. In the configuration shown, a B atom is on top of a surface Al atom (HCP-top-B configuration), and another atomic configuration can be generated by swapping B and N atoms in the lattice (HCP-top-N configuration).

vacancy defects is described through vacancy formation energy, E_f, defined as

$$E_f[X] = E[X] - E[\text{pristine}] + \mu_X \quad (2)$$

where $E[X]$ and $E[\text{pristine}]$ are the total energies of the system with a missing atom (X = B or N for h-BN) and the pristine system (either on metal substrate or free-standing), respectively, and μ_X is the chemical potential of the missing atom in the reference system. For h-BN, in thermodynamic equilibrium

$$\mu_{BN} = \mu_B + \mu_N \quad (3)$$

and as we are interested not in estimating the equilibrium concentration of defects but in assessing the bonding between h-BN sheet with defects and Al surface, we do not correlate the chemical potentials with the experimental conditions. Instead, we assume that μ_N is the same as in a N_2 molecule (N-rich conditions) as in previous works[33,34] and use eq 3 to evaluate μ_B.

Calculations for a free-standing h-BN sheet gave $E_f[B] = 7.7$ eV and $E_f[N] = 7.8$ eV for the neutral charge state of the vacancies. These values are in a good agreement with the results of previous calculations (7−9 eV).[35−40] For the h-BN/Al system, the situation is more complicated. Vacancy formation energies will depend on the position of the defect in the moiré pattern.

Figure 4 shows the atomic structure of the interface and the supercell used in our calculations. Al atoms are represented as balls colored according to their depth with regard to the surface. There are several high-symmetry atomic positions at the interface between h-BN and Al(111). The centers of BN-hexagons can be associated with the HCP, FCC positions in the underlying Al lattice, as well as with the TOP position (on top of a surface Al atom). In the configuration shown in Figure 4, a boron atom is on top of a surface aluminum atom (HCP-top-B configuration), and another atomic configuration can be generated by swapping B and N atoms in the lattice (HCP-top-N configuration). For either configuration, there are 64 inequivalent positions of B atoms and 64 inequivalent positions of N atoms where vacancies can be created. To avoid unrealistically large computations, we concentrate on the limiting cases, i.e., vacancies created in high-symmetry areas at the interface, because energies of defects in the intermediate positions are expected to be within the energies corresponding to the liming cases. We will use the following notations: HCP-top-B means that a B vacancy was created in the HCP area in the top position of the B atom, and FCC-hcp-B means that B vacancy was created in the FCC area in the position of the hcp atom, etc. All defects were considered to be in the neutral charge state, as the presence of the Al matrix should eliminate the possibility of localized charges.

To characterize the interaction strength between h-BN and Al surface in the presence of defects, it is instructive, in addition to E_f, described by eq 2, to introduce defect-induced interaction energy $E_i[X]$

$$E_i[X] = E[\text{Al} + \text{BN}; X] - (E[\text{Al}] + E[\text{BN}; X]) - E_b^{\text{tot}} \quad (4)$$

where $E[\text{Al+BN}; X]$ is the total energy of the h-BN/Al system with a vacancy in the h-BN atomic network (X = B or N for h-BN), and $E[\text{Al}]$ and $E[\text{BN}; X]$ are the total energies of the isolated Al slab and h-BN with the vacancy. E_b^{tot} is the vdW energy for the whole supercell without defects, eq 1. Thus, $E_i[X] = 0$ if no additional interaction comes from the defect.

The results of the calculations are presented in Table 1. The typical atomic geometries are shown in Figure 5. It is evident that while N-vacancies do not give rise to any sizable interaction between the h-BN sheet and Al surface, B-vacancies interact strongly with the Al. The highly reactive N atoms with dangling bonds essentially "pull out" the underlying Al atom from the surface, thus "plugging" the hole. However, the Al

dx.doi.org/10.1021/jp509505j | J. Phys. Chem. C 2014, 118, 26894−26901

Table 1. Vacancy Formation Energies in h-BN Sheet, E_f, along with the Interaction Energy, E_i, and Critical Shear Stress, τ_c, for Defect Concentration of 0.78%

defect type	E_f (eV)	E_i (eV)	τ_c (MPa)
B-vacancy, free-standing	7.7	–	–
N-vacancy, free-standing	7.8	–	–
HCP-top-B configuration			
pristine interface	–	–	~10
TOP-hcp-N	7.7	−0.3	~20
TOP-fcc-B	4.7	−2.4	220
FCC-top-N	7.7	−0.3	~20
FCC-hcp-B	1.6	−5.5	450
HCP-top-B	0.2	−6.8	210
HCP-fcc-N	7.4	−0.6	~20
HCP-top-N configuration			
pristine interface	–	–	~10
TOP-hcp-B	−0.4	−7.4	225
TOP-fcc-N	7.6	−0.4	~20
FCC-top-B	−0.1	−7.2	210
FCC-hcp-N	7.7	−0.3	~20
HCP-top-N	7.7	−0.3	~20
HCP-fcc-B	−0.5	−7.6	205

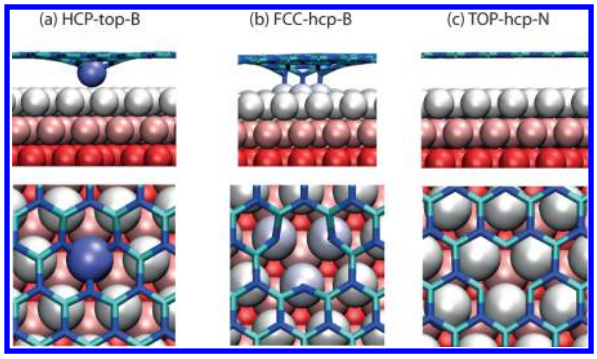

Figure 5. Typical atomic configurations of B (a,b) and N (c) vacancies at the h-BN/Al interface for the HCP-top-B configuration, shown in Figure 4. The interaction of B vacancies with surface Al atoms is very strong, whereas N vacancies do not interact with the Al surface atoms. The Al atoms represented as big balls are colored according to the elevation.

atomic radius is larger than that of B (125 versus 85 pm), and the Al atom cannot replace the missing B atom; it is "too big", so that it is "protruding" from the h-BN sheet. The reason for such a behavior is a very small formation energy of a surface vacancy on the (111) Al surface, 0.53 eV, as our calculations indicate, and the isoelectronic structure of Al atom ($3s^2 3p^1$) with respect to B ($2s^2 2p^1$), as immediately evident from the atom locations in the periodic table. The absolute values (especially negative ones) should be treated with caution, as they depend on the choice of the reference chemical potential of the atoms, but the trend is clear: interaction between the h-BN sheet with B-vacancies and Al atoms is strong, and defect formation energy decreases considerably. A drop in vacancy formation energies has also been reported for vacancies in h-BN[31] and graphene[28] on transition metals. This does not mean, however, that the adhesion of the h-BN sheet increases as much as E_i indicates. If the h-BN sheet is moved up away from the surface, the protruding Al atom will easily follow. In fact, the interaction energy, E_i^*, defined as a difference between the h-BN sheet with the Al atom in the B position and Al slab with a surface vacancy SV, is only 0.6 eV for the HCP-top-B configuration.

Having evaluated the energy of B/N vacancy formation at the h-BN/Al interface, we proceed to calculations of critical shear stress, τ_c, using the same simulation setup as for the pristine system. Such calculations are meaningful only for a certain defect concentration, which was 0.78% in our case. N vacancies did not change τ_c much, as one can expect from the atomic configuration at the interface. However, B-vacancy gives rise to an increase in τ_c. The typical values for the lowest-energy configuration defects, such as HCP-top-B, proved to be about 200 MPa. The simulations showed that the pulled-out Al atom follows the h-BN sheet giving rise to additional interaction between the h-BN sheet and the metal. As for the FCC-hcp-B configuration, once a potential barrier is overcome (which gives rise to a higher value of τ_c), it transforms to a configuration similar to that presented in Figure 5a.

Larger Vacancy Defects: Tetra Vacancies. We also considered several larger defects, such as tetra vacancies. The typical atomic configuration of a tetra vacancy with one missing N and three missing B atoms at the h-BN/Al interface is shown in Figure 6a. Such triangular defects with double-coordinated N

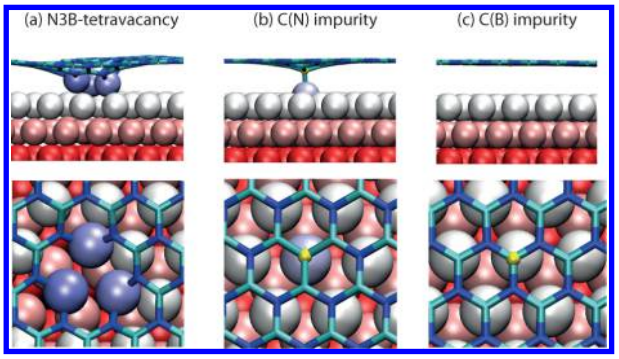

Figure 6. (a) Typical atomic configuration of a tetra vacancy with one missing N and 3B atoms at the h-BN/Al interface. Similar to B single vacancies, the interaction of such tetra vacancies with Al atoms is very strong. The Al atoms represented as big balls are colored according to the elevation. In the diagram of atomic structure of the h-BN/Al interface with C atoms in the substitutional N (b) and B (c) positions, the C atom is shown as a small yellow ball. The C(N) impurity gives rise to covalent bonding between the h-BN sheet and Al surface.

atoms at the edges have been observed in TEM images of BN sheets.[41,42] Similar to B single vacancies, the interaction of the tetra vacancies having double-coordinated N atoms at the edges with Al atoms is very strong, so that three surface atoms are pulled out from the surface, reducing the formation energy of the defect. Such defects also exhibit higher values of $\tau_c \sim 300$ MPa. We did not find substantial covalent interaction between tetra vacancies with undercoordinated B atoms at the edges and Al surface.

Substitutional C Impurities in N and B Positions. Finally, as substitutional C impurities are frequently present in h-BN systems[43] or can deliberately be introduced by electron-beam-irradiation-mediated techniques[44,45] or direct ion implantation,[46] we studied how such impurities affect the bonding. We found that whereas C atoms in the B atom positions do not give rise to covalent bonding, a single C atom in the N position forms a covalent bond with the surface with a binding energy of 2.0 eV. Our simulations also showed that $\tau_c = 210$ MPa, and the BN sheet with the C atom does not pull any Al atom when

dx.doi.org/10.1021/jp509505j | J. Phys. Chem. C 2014, 118, 26894−26901

moving parallel to the surface, but rebonding of the C atom with the equivalent surface Al atom occurs.

Mechanical Properties of h-BN Sheets with Point Defects and Dependence of Critical Shear Stress on Defect Concentration. As defects normally give rise to deterioration of mechanical properties of materials, we finally assessed the effects of vacancies and substitutional defects on the in-plane stiffness C of h-BN, calculated using

$$C = \frac{1}{S_0}\frac{\partial^2 E}{\partial \varepsilon^2} \quad (5)$$

where S_0 is area of the 2D supercell, E the strain energy, and ε the strain in armchair direction. As partial derivatives at zero strain in other dimensions vanish, C can be referred to as an analog of the elastic constant C_{11} of bulk h-BN.[47] It is closely related to the Young's modulus of BNNTs.

For the pristine system we obtained a value of C = 257 N/m, which is in a good agreement with previously reported values.[47] The results are presented in Figure 7. As evident from the

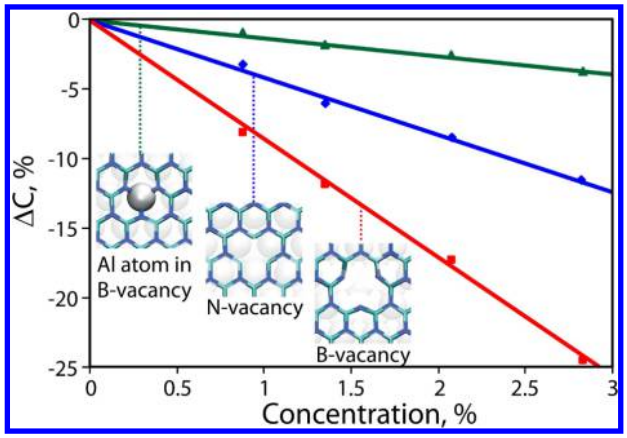

Figure 7. In-plane stiffness C of h-BN with various defects as a function of defect concentration. Triangles, diamonds, and squares correspond to h-BN sheet with Al impurity in the position of a B-vacancy, with naked N-vacancy, and with B-vacancy, respectively. The lines are guides for the eye.

curves, vacancy defects at concentrations up to 3% give rise to a drop in C of about 11% and 24% for N- and B-vacancies, respectively; however, for the energetically favorable configurations in which Al atoms are bonded to BN sheets with vacancies, Figure 5, a drop of only 2% was observed. Such negligible changes in C allow us to conclude that if such type of vacancies dominates, h-BN materials with defects will display practically the same stiffness as the pristine material and can therefore be used for reinforcing the aluminum matrix, provided that the concentration of other defects, e.g., N-vacancies, is small. Changes of the same order of magnitude should be expected for the BNNT Young's modulus. On the basis of the results for carbon nanotubes,[48] a somewhat stronger effect of vacancies on tensile strength of BNNTs can be anticipated, but even if tensile strength decreases by a factor of 2, it will still be considerably higher than that of Al matrix.

Assuming that the defects at the Al/BN interface provide $\tau_c \sim 200$ MPa at a defect concentration of n = 0.78% and that there is a linear relationship between τ_c and n, which should hold until defects start overlapping, at $n \sim 6\%$, one can expect $n_c \sim 1.5$ GPa, which may be sufficient to provide good mechanical characteristics of the interface without excessive damage of BNNTs. In practice, an "optimum" amount of defects should exist, as during the reinforcement of carbon nanotube bundles by controllable introduction of defects using electron beam irradiation.[49,50] It should also be pointed out that BNNTs always have intershell links, which provide mechanical load transfer to the inner shells of the BNNTs. It is also worth noting that in practice other than (111) surfaces should be present at the Al−BN interface. As high-index surfaces of FCC metals are more reactive, this should make the bonding and critical shear stress even higher. We emphasize that the critical shear stress calculated in our work is one of the most important parameters in various macroscopic models of nanotube-metal composites[3] or nanotube networks.[51]

In practice, the defects at the surface of BNNTs can be created by plasma (in particular, B plasma) or chemical treatment. For laboratory samples with nano dimensions, beams of energetic ions can also be used after the composites have been made. The oxidation of Al and other impurities at the interface and formation of new phases at the interface may make the picture more complicated, but the overall effect of defects at the interface should be beneficial on the mechanical characteristics of macroscopic Al−BNNTs composite materials.

CONCLUSIONS

Using first-principles DFT calculations with advanced XC functionals which account for vdW interaction, we studied the morphology and energetics of the atomic interface between BNNTs Al matrix. We found that for the ideal interface the bonding energy and the critical shear stress are quite small, of the order of 15 meV/Å^2 and 20 MPa, respectively, as corroborated by our experimental data. We further assessed how point defects such as atomic vacancies and substitutional impurities affect the interface bonding. We showed that some point defects, e.g., single B vacancies, change dramatically the interface structure and increase the bonding as well as critical shear stress. At a defect concentration of about 6%, the critical shear stress can be of the order of 1.5 GPa, which may be sufficient to provide good mechanical characteristics of the interface without excessive deterioration of the mechanical properties of the BNNTs. Larger vacancies and substitutional C impurities in the BN sheets have a stronger effect on the adhesion. The critical shear stress and mechanical characteristics of BNNTs with defects, calculated in our work as functions of defect concentration, can be used as basic input parameters in various macroscopic models of Al/BNNTs composites. The weak dependence of the in-plane h-BN stiffness upon concentration of vacancies with Al atoms in the positions of missing B atoms in a range of up to 3% indicates that BNNT will display practically the same stiffness in h-BN/Al composites and therefore can reinforce the Al matrix. Overall, our theoretical results explain the weak bonding at the interface between pristine BNNTs and Al and suggest new ways for the development of nanostructured BN−Al materials with improved mechanical characteristics.

AUTHOR INFORMATION

Corresponding Author

*E-mail: arkady.krasheninnikov@aalto.fi.

Notes

The authors declare no competing financial interest.

■ ACKNOWLEDGMENTS

The work was carried out with partial financial support from the Ministry of Education and Science of the Russian Federation in the framework of Increase Competitiveness Program of NUST "MISiS" (K3-2014-010). D.G. also acknowledges a "Mega-Grant" award for leading scientists tenable at the National University of Science and Technology "MISIS", Moscow, Russian Federation, under Agreement 11.G34.31.0061. D.G.K. acknowledges the support from the Russian Ministry of Education and Science (948 from 21 of November 2012). A.V.K. also acknowledges financial support from the Academy of Finland through Project 263416. N.B., T.B., and R.M.N. further thank the Academy of Finland for the support through its Centres of Excellence Programme (2012-2017) under Project 251748. We also thank CSC-IT Center for Science Ltd. for generous grants of computer time.

■ REFERENCES

(1) Tsuia, T. Y.; Olivera, W. C.; Pharra, G. M. Influences of stress on the measurement of mechanical properties using nanoindentation: Part I. Experimental studies in an aluminum alloy. *J. Mater. Res.* **1996**, *11*, 752−759.

(2) Polmear, I. *Light Alloys: Metallurgy of the Light Metals*, 3rd ed.; Butterworth-Henemann: Oxford, 1995.

(3) Bakshi, S.; Lahiri, D.; Agarwal, A. Carbon nanotube reinforced metal matrix composites − A review. *Int. Mater. Rev.* **2010**, *55*, 41−64.

(4) Laha, T.; Agarwal, A.; McKechnie, T.; Seal, S. Synthesis and characterization of plasma spray formed carbon nanotube reinforced aluminum composite. *Mater. Sci. Eng., A* **2004**, *381*, 249−258.

(5) Kuzumaki, T.; Miyazawa, K.; Ichinose, H.; Ito, K. Processing of Carbon Nanotube Reinforced Aluminum Composite. *J. Mater. Res.* **1998**, *13*, 2445−2449.

(6) Jorio, A.; Dresselhaus, G.; Dresselhaus, M. In *Carbon Nanotubes: Advanced Topics in the Synthesis, Structure, Properties and Applications*; Jorio, A., Dresselhaus, G., Dresselhaus, M., Eds.; Topics in Applied Physics; Springer: New York, 2008; Vol. *111*.

(7) Golberg, D.; Bando, Y.; Huang, Y.; Terao, T.; Mitome, M.; Tang, C.; Zhi, C. Boron nitride nanotubes and nanosheets. *ACS Nano* **2010**, *4*, 2979−93.

(8) Salas, W.; Alba-Baena, N. G.; Murr, L. E. Explosive Shock-Wave Consolidation of Aluminum Powder/Carbon Nanotube Aggregate Mixtures: Optical and Electron Metallography. *Metall. Mater. Trans. A* **2007**, *38A*, 2928−2935.

(9) Yamaguchi, M.; Tang, D.-M.; Zhi, C.; Bando, Y.; Shtansky, D.; Golberg, D. Synthesis, structural analysis and in situ transmission electron microscopy mechanical tests on individual aluminum matrix/boron nitride nanotube nanohybrids. *Acta Mater.* **2012**, *60*, 6213−6222.

(10) Yamaguchi, M.; Bernhardt, J.; Faerstein, K.; Shtansky, D.; Bando, Y.; Golovin, I. S.; Sinning, H.-R.; Golberg, D. Fabrication and characteristics of melt-spun Al ribbons reinforced with nano/micro-BN phases. *Acta Mater.* **2013**, *61*, 7604−7615.

(11) Yamaguchi, M.; Meng, F.; Firestein, K.; Tsuchiya, K.; Golberg, D. Powder metallurgy routes toward aluminum boron nitride nanotube composites, their morphologies, structures and mechanical properties. *Mater. Sci. Eng., A* **2014**, *604*, 9−17.

(12) Corso, M.; Auwarter, W.; Muntwiler, M.; Tamai, A.; Greber, T.; Osterwalder, J. Boron Nitride Nanomesh. *Science* **2004**, *303*, 217−220.

(13) Song, L.; Ci, L.; Lu, H.; Sorokin, P. B.; Jin, C.; Ni, J.; Kvashnin, A. G.; Kvashnin, D. G.; Lou, J.; Yakobson, B. I.; et al. Large Scale Growth and Characterization of Atomic Hexagonal Boron Nitride Layers. *Nano Lett.* **2010**, *10*, 3209−3215.

(14) Joshi, S.; Ecija, D.; Koitz, R.; Iannuzzi, M.; Seitsonen, A.; Hutter, J.; Sachdev, H.; Vijayaraghavan, S.; F, B.; Seufert, K.; et al. Boron Nitride on Cu(111): An Electronically Corrugated Monolayer. *Nano Lett.* **2012**, *12*, 5821−5828.

(15) Cavar, E.; Westerstrom, R.; Mikkelsen, A.; Lundgren, E.; Vinogradov, A.; Ng, M. L.; Preobrajenski, A.; Zakharov, A.; Martensson, N. A single h-BN layer on Pt. *Surf. Sci.* **2008**, *602*, 1722−1726.

(16) Müller, F.; Hüfner, S.; Sachdev, H.; Laskowski, R.; Blaha, P.; Schwarz, K. Epitaxial growth of hexagonal boron nitride on Ag(111). *Phys. Rev. B: Condens. Matter Mater. Phys.* **2010**, *82*, 113406.

(17) Preobrajenski, A.; Nesterov, M.; Ng, M. L.; Vinogradov, A.; Martensson, N. Monolayer h-BN on lattice-mismatched metal surfaces: On the formation of the nanomesh. *Chem. Phys. Lett.* **2007**, *446*, 119−123.

(18) Gómez Díaz, J.; Ding, Y.; Koitz, R.; Seitsonen, A. P.; Iannuzzi, M.; Hutter, J. Hexagonal boron nitride on transition metal surfaces. *Theor. Chem. Acc.* **2013**, *132*, 1350.

(19) Kresse, G.; Furthmüller, J. Efficiency of ab-initio total energy calculations for metals and semiconductors using a plane-wave basis set. *Comput. Mater. Sci.* **1996**, *6*, 15−50.

(20) Kresse, G.; Furthmüller, J. Efficient iterative schemes for ab initio total-energy calculations using a plane-wave basis set. *Phys. Rev. B: Condens. Matter Mater. Phys.* **1996**, *54*, 11169−11186.

(21) Blöchl, P. E. Projector augmented-wave method. *Phys. Rev. B: Condens. Matter Mater. Phys.* **1994**, *50*, 17953−17979.

(22) Vydrov, O. A.; Voorhis, T. V. Nonlocal van der Waals density functional: The simpler the better. *J. Chem. Phys.* **2010**, *133*, 244103.

(23) Björkman, T. van der Waals density functional for solids. *Phys. Rev. B: Condens. Matter Mater. Phys.* **2012**, *86*, 165109.

(24) Enkovaara, J.; Rostgaard, C.; Mortensen, J. J.; Chen, J.; Dułak, M.; Ferrighi, L.; Gavnholt, J.; Glinsvad, C.; Haikola, V.; Hansen, H. A.; et al. Electronic structure calculations with GPAW: a real-space implementation of the projector augmented-wave method. *J. Physics: Condensed Matter* **2010**, *22*, 253202.

(25) Dion, M.; Rydberg, H.; Schröder, E.; Langreth, D. C.; Lundqvist, B. I. Van der Waals Density Functional for General Geometries. *Phys. Rev. Lett.* **2004**, *92*, 246401.

(26) Golberg, D.; Mitome, M.; Bando, Y.; Tang, C. Multi-walled boron nitride nanotubes composed of diverse cross-section and helix type shells. *Appl. Phys. A: Mater. Sci. Process.* **2007**, *88*, 347−352.

(27) Busse, C.; Lazić, P.; Djemour, R.; Coraux, J.; Gerber, T.; Atodiresei, N.; Caciuc, V.; Brako, R.; N'Diaye, A.; Blügel, S.; et al. Graphene on Ir(111): Physisorption with Chemical Modulation. *Phys. Rev. Lett.* **2011**, *107*, 036101.

(28) Standop, S.; Lehtinen, O.; Herbig, C.; Lewes-Malandrakis, G.; Craes, F.; Kotakoski, J.; Michely, T.; Krasheninnikov, A. V.; Busse, C. Ion impacts on graphene/Ir(111): Interface channeling, vacancy funnels, and a nanomesh. *Nano Lett.* **2013**, *13*, 1948−55.

(29) Blanc, N.; Jean, F.; Krasheninnikov, A. V.; Renaud, G.; Coraux, J. Strains Induced by Point Defects in Graphene on a Metal. *Phys. Rev. Lett.* **2013**, *111*, 085501.

(30) Björkman, T.; Gulans, A.; Krasheninnikov, A.; Nieminen, R. van der Waals Bonding in Layered Compounds from Advanced Density-Functional First-Principles Calculations. *Phys. Rev. Lett.* **2012**, *108*, 235502.

(31) Cun, H.; Iannuzzi, M.; Hemmi, A.; Osterwalder, J.; Greber, T. Two-Nanometer Voids in Single-Layer Hexagonal Boron Nitride: Formation via the "Can-Opener" Effect and Annihilation by Self-Healing. *ACS Nano* **2014**, *8*, 7423−31.

(32) McCarthy, B.; Coleman, J. N.; Czerw, R.; Dalton, A. B.; in het Panhuis, M.; Maiti, A.; Drury, A.; Bernier, P.; Nagy, J. B.; Lahr, B.; et al. A Microscopic and Spectroscopic Study of Interactions between Carbon Nanotubes and a Conjugated Polymer. *J. Phys. Chem. B* **2002**, *106*, 2210−2216.

(33) Schmidt, T. M.; Baierle, R. J.; Piquini, P.; Fazzio, A. Theoretical study of native defects in BN nanotubes. *Phys. Rev. B: Condens. Matter Mater. Phys.* **2003**, *67*, 113407.

(34) Berseneva, N.; Krasheninnikov, A. V.; Nieminen, R. M. Mechanisms of Postsynthesis Doping of Boron Nitride Nanostructures with Carbon from First-Principles Simulations. *Phys. Rev. Lett.* **2011**, *107*, 035501.

(35) Azevedo, S.; Kaschny, J. R.; de Castilho, C. M. C.; de Brito Mota, F. A theoretical investigation of defects in a boron nitride monolayer. *Nanotechnology* **2007**, *18*, 495707.
(36) Zobelli, A.; Ewels, C.; Gloter, A.; Seifert, G.; Stephan, O.; Csillag, S.; Colliex, C. Defective Structure of BN Nanotubes: From Single Vacancies to Dislocation Lines. *Nano Lett.* **2006**, *6*, 1955−1960.
(37) Orellana, W.; Chacham, H. Stability of native defects in hexagonal and cubic boron nitride. *Phys. Rev. B: Condens. Matter Mater. Phys.* **2001**, *63*, 125205.
(38) Yin, L.-C.; Cheng, H.-M.; Saito, R. Triangle defect states of hexagonal boron nitride atomic layer: Density functional theory calculations. *Phys. Rev. B: Condens. Matter Mater. Phys.* **2010**, *81*, 153407.
(39) Huang, B.; Lee, H. Defect and impurity properties of hexagonal boron nitride: A first-principles calculation. *Phys. Rev. B: Condens. Matter Mater. Phys.* **2012**, *86*, 245406.
(40) Machado-Charry, E.; Boulanger, P.; Genovese, L.; Mousseau, N.; Pochet, P. Tunable magnetic states in hexagonal boron nitride sheets. *Appl. Phys. Lett.* **2012**, *101*, 132405.
(41) Jin, C.; Lin, F.; Suenaga, K.; Iijima, S. Fabrication of a Freestanding Boron Nitride Single Layer and Its Defect Assignments. *Phys. Rev. Lett.* **2009**, *102*, 195505.
(42) Meyer, J. C.; Chuvilin, A.; Algara-Siller, G.; Biskupek, J.; Kaiser, U. Selective Sputtering and Atomic Resolution Imaging of Atomically Thin Boron Nitride Membranes. *Nano Lett.* **2009**, *9*, 2683−2689.
(43) Krivanek, O. L.; Chisholm, M. F.; Nicolosi, V.; Pennycook, T. J.; Corbin, G. J.; Dellby, N.; Murfitt, M. F.; Own, C. S.; Szilagyi, Z. S.; Oxley, M. P.; et al. Atom-by-atom structural and chemical analysis by annular dark-field electron microscopy. *Nature (London, U.K.)* **2010**, *464*, 571−574.
(44) Wei, X.; Wang, M.; Bando, Y.; Golberg, D. Electron-Beam-Induced Substitutional Carbon Doping of Boron Nitride Nanosheets, Nanoribbons, and Nanotubes. *ACS Nano* **2011**, *5*, 2916−2922.
(45) Wei, X.; Wang, M.; Bando, Y.; Golberg, D. Post-Synthesis Carbon Doping of Individual Multiwalled Boron Nitride Nanotubes via Electron-Beam Irradiation. *J. Am. Chem. Soc.* **2010**, *132*, 13592−13593.
(46) Bangert, U.; Pierce, W.; Kepaptsoglou, D. M.; Ramasse, Q.; Zan, R.; Gass, M. H.; Van den Berg, J. A.; Boothroyd, C. B.; Amani, J.; Hofsäss, H. Ion Implantation of Graphene—Toward IC Compatible Technologies. *Nano Lett.* **2013**, *13*, 4902−7.
(47) Kudin, K. N.; Scuseria, G. E.; Yakobson, B. I. C_2F, BN, and C nanoshell elasticity from ab initio computations. *Phys. Rev. B: Condens. Matter Mater. Phys.* **2001**, *64*, 235406.
(48) Sammalkorpi, M.; Krasheninnikov, A.; Kuronen, A.; Nordlund, K.; Kaski, K. Mechanical properties of carbon nanotubes with vacancy-like defects. *Phys. Rev. B: Condens. Matter Mater. Phys.* **2004**, *70*, 245416.
(49) Kis, A.; Csányi, G.; Salvetat, J.-P.; Lee, T.-N.; Couteau, E.; Kulik, A. J.; Benoit, W.; Brugger, J.; Fórro, L. Reinforcement of single-walled carbon nanotube bundles by intertube bridging. *Nat. Mater.* **2004**, *3*, 153−157.
(50) Sammalkorpi, M.; Krasheninnikov, A. V.; Kuronen, A.; Nordlund, K.; Kaski, K. Irradiation-induced stiffening of carbon nanotube bundles. *Nucl. Instrum. Methods Phys. Res., Sect. B* **2005**, *228*, 142.
(51) Åström, J. A.; Krasheninnikov, A. V.; Nordlund, K. Carbon nanotube mats and fibers with irradiation-improved mechanical characteristics: A theoretical model. *Phys. Rev. Lett.* **2004**, *93*, 215503.